Hindawi
Advances in Materials Science and Engineering
Volume 2022, Article ID 3282211, 9 pages
https://doi.org/10.1155/2022/3282211

Research Article

Study on Bond Defect Detection in Grouted Rock Bolt Systems under Pullout Loads

Shuisheng Yu,[1,2] **Leilei Niu**,[2] **Jin Chen**,[3] **Yawei Wang**,[1] **and Honghao Yang**[1]

[1]*School of Architectural Engineering, Zhongyuan University of Technology, Zhengzhou 450007, China*
[2]*Center for Rock Instability and Seismicity Research, Department of Mining Engineering, School of Resource and Civil Engineering, Northeastern University, Shenyang 110819, China*
[3]*School of Economics and Management, Zhongyuan University of Technology, Zhengzhou 450007, China*

Correspondence should be addressed to Shuisheng Yu; yuss.1987@163.com

Received 3 June 2022; Accepted 18 August 2022; Published 31 August 2022

Academic Editor: Guosong Wu

In grouted rock bolt systems, bond defects often occur, which seriously affects the safety of rock mass structures. Therefore, in this study, based on the existence of bond defects, laboratory tests were conducted to detect the location and length of bond defects and study the guided wave propagation in grouted rock bolt systems under different pullout loads. The guided wave signal was analysed in the time domain and frequency domain. In addition to the laboratory test, a numerical simulation of the effect of different bond defect locations on ultrasonic guided wave propagation in rock bolts was conducted using a damage-based model. The influence mechanism of bond defects on guided wave propagation under different pullout loads was explored. The study confirmed that there existed a stress platform in the rock bolt at the bond defect under a pullout load. The location and length of the bond defect could be detected by the stress platform and guided wave. The debonding length increased exponentially with the amplitude ratio (Q) of low frequency to high frequency, and the Q value could be used as the quantitative index of debonding length. As the pullout load increased, the impedance mismatch between the rock bolt and cement mortar (defect) increased, and the guided wave propagation in grouted rock bolt systems was irregular. The pullout load weakened the guided wave propagation law. The larger the pullout load is, the greater the weakening effect is.

1. Introduction

As a part of support methods, rock bolt support is extensively used in both civil and mining engineering [1]. In actual rock bolt construction, construction quality problems inevitably exist, such as bond defects between rock bolts and anchor agents [2–4], insufficient lengths of rock bolts [5] and bolt corrosion [6–8], or the existence of natural joints in rock mass structures [9–11], which seriously affects the safety of rock mass structures. Therefore, addressing the problem of bond defects between rock bolts and anchor agents, Zhao and Yang [2] theoretically analysed the distribution of axial stress and shear stress in rock bolts with one bond defect. Xu et al. [3] analysed the distribution of axial stress and shear stress in a rock bolt with bond defects by test and numerical simulation, and the location of bond defects was determined. However, due to the time consumption and destructiveness of this method of studying concealed rock bolts, many scholars have conducted nondestructive testing (NDT) of rock bolts by ultrasonic guided waves or stress waves [5, 12–20]. Cui and Zou [5] studied the attenuation of ultrasonic guided waves in grouted rock bolts using numerical simulation and confirmed the influence of the insufficient length of rock bolts and the lack of mortar on grouted rock bolts and then verified it by testing. Han et al. [13] evaluated the integrity of rock bolts by ultrasonic guided waves. The results indicated that the guided wave velocity (here, guided wave velocity refers to the guided wave group velocity, which is the propagation velocity of the wave packet envelope in the medium and represents the propagation velocity of energy) increased with an increasing defect ratio. Yu et al. [15, 16] used the hammer impact method to evaluate the grouted ratio of rock bolts and pipe roof support systems under different bond lengths. The results indicated that the

hammer impact method could evaluate the bond length in the field. Li et al. [20] studied the propagation characteristics of ultrasonic guided waves in free bolts and full-length bonding resin bolts through theoretical analysis and experiments.

From the above studies, we can find that many scholars performed NDT on rock bolts only in the absence of loading. In actual projects, the environment of a deep rock mass is complicated and in three "high" states and one "disturbance" state (high ground stress, high karst water pressure, high earth temperature, and mining disturbance) [21]. It is accompanied by the process of mining and the impact of blasting load [22], resulting in rockburst, water inrush, and goaf instability, causing the stress acting on the rock bolt to change correspondingly. Because of the concealment of rock bolts, it is inappropriate to ignore the effect of stress levels on the detection of bond defects when using the NDT method. Considering the stress, Ivanovic et al. [23] conducted NDT on bolts to determine the variation in the frequency response with a change in prestressing. Ivanovic and Neilson [24] used magnetostrictive NDT to assess the effective total bolt length under different prestress loads. However, there are no bond defects in their models [23, 24]. In practice, bond defects often exist in grouted rock bolt systems, and it is necessary to detect the location and length of bond defects under various stress levels to ensure safety and avoid accidents in grouted rock bolt systems.

Therefore, in this study, a laboratory test of grouted rock bolt systems with one bond defect was conducted. The bond defect in grouted rock bolt systems was detected, and the propagation characteristic of ultrasonic guided waves under pullout loads was analysed. The effect of the pullout load on the guided wave propagation in grouted rock bolt systems with different bond defects was explored.

2. Test Arrangement

2.1. Specimen Design. Ribbed rock bolts with a diameter of 25 mm were grouted in concrete, which was used to simulate the rock mass. The diameter and length of the concrete specimen were 150 and 1,500 mm, respectively. The total length of the rock bolt was 2,500 mm, of which only 1,500 mm was grouted in the concrete specimen. There is a 400 mm defect 400 mm away from the B-end. The details of the rock bolt specimens are shown in Figure 1.

The surrounding rock was simulated using C40 concrete. The raw materials used for the concrete specimens were as follows: (1) ordinary Portland cement with a standard 28-day compressive strength of 42.5 MPa made by Shenyang Shanshui Gongyuan Cement Co., Ltd. (China); (2) Shenyang tap water; (3) fine aggregates of natural river sand with diameters from 0.3 to 1.18 mm; (4) coarse aggregates of cobblestone with diameters from 5 to 20 mm. The mix proportions of the concrete specimens used in this study were cement:water:fine aggregate:coarse aggregate = 1 : 0.47 : 1.3 : 3.02.

Cement mortar was used as the anchor agent. The raw materials used for cement mortar were as followa: (1) ordinary Portland cement with a standard 28-day compressive strength of 42.5 MPa; (2) tap water; (3) fine aggregates of natural river sand with diameters from 0.3 to 0.6 mm.

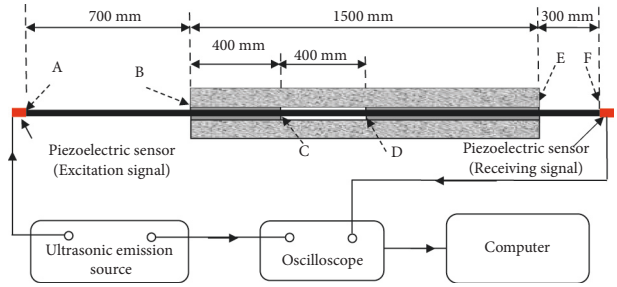

Figure 1: Grouted rock bolt systems model with one bond defect.

To ensure slip occurred before the bolt shank failed and the ease of pouring cement mortar into the boreholes, the mix proportions of cement mortar used in this study were cement:water:fine aggregate = 1 : 1 : 3.2. The mix proportions of cement mortar and concrete in the test are shown in Table 1.

To simulate the test in the field, the procedures for making specimens were as follows. First, a plain round bar with a diameter of 40 mm was placed centrally in the cylindrical steel mould, and then concrete was cast and vibrated using a poker vibrator. After 48 h curing of the concrete, the plain round bar was pulled out, and the concrete specimen was taken out of the mould and cured for 28 days in the room. Then, the rock bolts were grouted centrally in the hole with cement mortar, a defect with a length of 400 mm was set 400 mm from the B-end (Figure 1), and pullout tests were carried out after 7 days.

2.2. Test Apparatus. A pullout testing machine (PTM) was designed and manufactured to conduct the rock bolt pullout test with monitoring of the stress wave propagation in the rock bolt [25, 26]. The pullout load was applied to the rock bolt by a hollow Jack with a 300 kN loading capacity, and the load was measured by a load transducer. Piezoelectric sensors (TH-GP) and ultrasonic emission sources (TH-F) were produced by Xiangtan Tianhong Testing Technology Co., Ltd. (China). The emission voltages of the ultrasonic emission source were 100–1,000 V. The piezoelectric sensor was used as the receiving or excitation sensor, which could excite 10-cycle sine wave packets with a main frequency of 22 kHz. The ultrasonic excitation sensor contacted the loading end (A-end in Figure 1) of the rock bolt through a coupling agent (such as Vaseline) and generated the signal that was received at the free end (F-end in Figure 1) of the rock bolt using the receiving sensor. Furthermore, a static strain indicator, digital oscilloscope, and computer were used in the test. All test data were stored in the computer. A schematic diagram of the PTM is shown in Figure 1.

The testing procedure was as follows. First, the grouted rock bolt was not subjected to axial force, and the ultrasonic excitation sensor was used to excite the ultrasonic guided wave at the A-end and was received by the receiving sensor at the F-end. Thereafter, the load was increased to 50 kN, and the above steps were repeated until the rock bolt was completely debonded.

Table 1: Mix proportions of concrete and cement mortar in a test.

Ingredient	Water	Cement	Sand	Stone
Concrete	0.47	1	1.3	3.02
Cement mortar	1	1	3.2	0

3. Experimental Results and Discussion

The relationship between the axial load and displacement of the rock bolt is shown in Figure 2. Due to the presence of bond defects in grouted systems and the short curing time of cement mortar, the rock bolt did not undergo plastic deformation. With increasing load, the interface between the rock bolt and cement mortar experienced elastic ascending, softening, and debonding stages.

Figure 3(a) presents the guided wave propagation characteristics under pullout load. In terms of signal time picking, some scholars [27, 28] adopt the time difference between peaks or troughs of signals, while other scholars [29] adopt the time difference between the starting points. In the test, one end is used to transmit the signal, and the signal is not recorded. The other end is used to receive and record the signal; therefore, the time difference between the starting points is used to pick up the first wave at the receiving end, while the time difference between the peaks or troughs can be used to pick up the subsequent echoes.

According to the results of previous tests, the wave velocity of the free rock bolt was 5,100m/s; therefore, the wave velocity of the rock bolt at the bond defect was also 5,100m/s. Under a 0 kN load, the bond between the rock bolt and the cement mortar was tight, and more guided wave energy leaked to the cement mortar and concrete, resulting in severe attenuation, and wave velocity decreased. The wave velocity in the bond section was 4,435m/s, the defect length could be calculated, namely, 391 mm, and the difference was 2.25% compared to the actual bond defect length of 400 mm. According to the reflection of the guided wave at the C-end (Figure 1) of the bond defect, we know that the distance from the C-end to the B-end was 430 mm, and the difference was 7.5% compared with the actual distance of 400 mm. When the rock bolt was completely debonded, the bond between the rock bolt and the cement mortar was loose, the interface between the rock bolt and the cement mortar relied only on friction to transfer force, and the attenuation of the guided wave energy in the rock bolt decreased. The wave velocity of the rock bolt in the bond section increased to 4 783m/s. Therefore, using the wave velocities of the free rock bolt, the rock bolt in the bond section without loading, and the rock bolt in the bond section after the rock bolt complete debonding, it could be determined that the debonding length of the rock bolt was 669 mm under a 50 kN load, and the average wave velocity was 4,647m/sin the bond section. Under a 50 kN load, the defect length was 379 mm according to the echo from the C-end and the D-end, and the difference was 5.25% compared to the actual bond defect length of 400 mm in grouted rock bolt systems.

Figure 3(b) presents the frequency domain of the guided wave under a pullout load, and there existed a low-frequency band and a high-frequency band in the propagation process

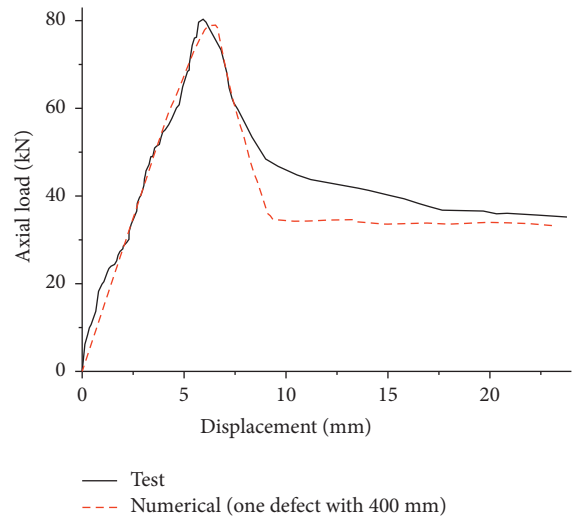

Figure 2: The relationship of axial load and displacement of rock bolt.

of the guided wave. In the low-frequency domain, the frequency of the guided wave at maximum amplitude under a 50 kN load was higher than that under a 0 kN load and rock bolt complete debonding. The result was in agreement with the study by Song and Cho [30], who found that the frequency of the stress wave in partly debonding shotcrete was greater than those in fully bonded and debonded states.

Due to the change in the grouted rock bolt state, the frequency in the rock bolt changes with load from 0 to 100 kN until the rock bolt completely debonds. Trtnik and Gams [31] set the frequency range of 0–50 kHz as the low-frequency region and 100–150 kHz as the high-frequency region according to the phenomenon that the low frequency of ultrasonic waves is concentrated in the 0–50 kHz region and the high-frequency region in the 100–150 kHz region in the test. The setting process of cement pastes was analysed by Trtnik and Gams [31] using the ratio of the difference between the maximum amplitudes and the sum of the maximum amplitudes in the high- and low-frequency regions of ultrasonic waves. Therefore, according to the experimental phenomenon, 0–30 kHz is set as the low-frequency region, while 50–70 kHz is set as the high-frequency region. The bond quality of the grouted rock bolt systems with bond defects can be quantitatively evaluated using the ratio of the maximum amplitude in the low-frequency region (F_{low}) and high-frequency region (F_{high}) (i.e., $Q = a_1/a_2$, where Q is the initial letter of quality). The load ranged from 0 to 50 kN, and until complete debonding of the rock bolt, the Q values were 2.85, 1.92, and 1.72. The relationship between the Q value and rock bolt debonding length is shown in Figure 4. With the increase in the Q value, the debonding length decreases exponentially, and the bond quality improves, and vice versa. Although the test data were limited, we used a variety of curves to fit the test data. The results showed that the exponential curve was the most consistent with the data.

The time-frequency domain of the guided wave under pullout loads is shown in Figure 3(c). There were 3 frequency distribution bands in the guided wave under 0 kN and 50 kN

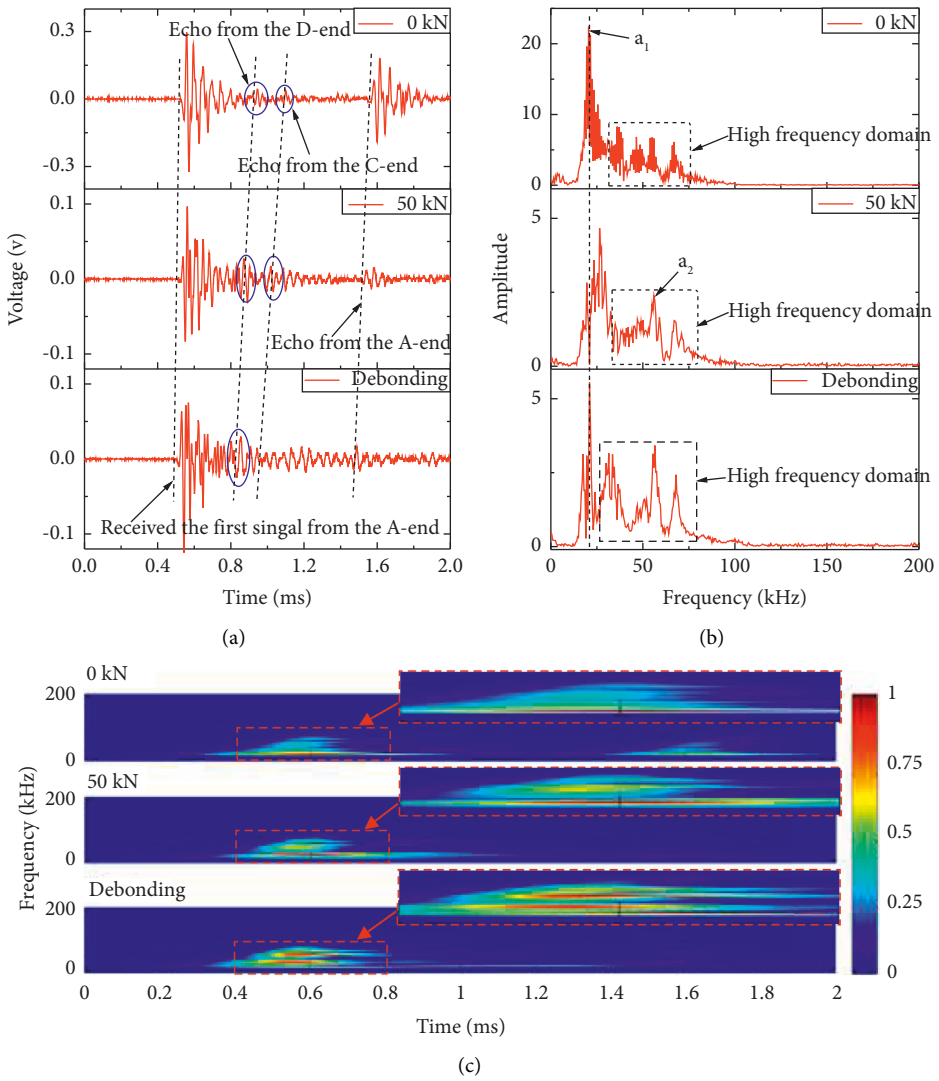

Figure 3: The wave propagation signal received at the F-end under pullout load, (a) Time domain; (b) frequency domain; (c) time-frequency domain.

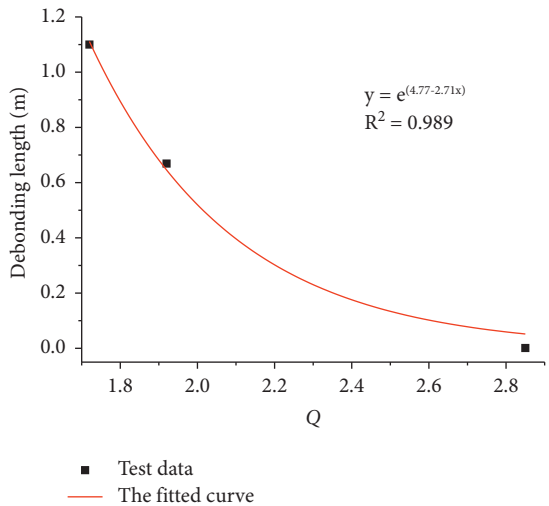

Figure 4: The relationship of Q value and debonding length.

loads and 4 frequency bands under rock bolt complete debonding. This phenomenon was in accordance with the results of Yao et al. [32] that found multiple frequency bands. In Figure 3(b), there were 5 frequency bands under a 0 kN load, which was inconsistent with the spectrogram in Figure 3(c). The colour of the spectrogram was basically similar and indistinguishable because of the approximately equal amplitudes of the 3 frequency bands. Under a 0 kN load, the frequency band ranges were 16–38 kHz, 41–58 kHz, and 62–72 kHz. In the low-frequency band, the colour of the spectrogram was the deepest, but those of the other 2 frequency bands were light. The centre frequency was mainly concentrated in the range of 17–23 kHz, and the duration range of this frequency band was 0.3–1 ms. The other time ranges were very difficult to observe because their amplitudes were much lower. Under a 50 kN load, the ranges of the frequency bands were 17–30 kHz, 37–59 kHz, and 65–76 kHz, while the spectrogram colour of the intermediate band was deeper than that of 0 kN. During the whole propagation process of the guided wave, the central

frequency distribution of the guided wave was mainly concentrated at 24–28 kHz, and the duration range of the frequency band became longer and was 0.3–1.2 ms. When the bolt was completely debonded, the ranges of the frequency bands were 16–22 kHz, 27–39 kHz, 46–61 kHz and 63–75 kHz, of which 3 bands were darker, and the distribution ranges were mainly 20–21 kHz, 29–36 kHz, and 53–60 kHz. The low-frequency band was concentrated in 20–21 kHz, the duration was greatest, and the range was 0.3–1.4 ms. The phenomenon of multiple frequency bands was related to the defects in grouted systems, and the guided wave had many reflections at the defect, which caused the frequency to change. From 0 kN to 50 kN load and until the rock bolt complete debonding, the guided wave energy leaked into the cement mortar and concrete decreased, the intensity of the high-frequency band increased, and the bond quality deteriorated. The A-end echo received at the F-end gradually weakened due to the effect of loading, which was consistent with the guided wave propagation signal in the rock bolt under the pullout load in Figure 3(a).

4. Numerical Analysis of Guided Wave Propagation in Grouted Rock Bolt Systems with Bond Defects

4.1. Numerical Simulation Theory and Experimental Verification

4.1.1. The Numerical Model of Grouted Rockbolt Systems. The numerical model was the same as the experimental model, and the distance from the C-end to the B-end was 400 mm with a bond defect length of 400 mm (Figure 1). The concrete damage plasticity model (CDPM) we used to simulate the mechanical behaviour of quasibrittle materials (concrete and cement mortar) was proposed for introduction to Abaqus by Lee and Fenves [33]. The CDPM takes into consideration isotropic damaged elasticity in combination with isotropic tensile and compressive plasticity to represent the inelastic behaviour of concrete [34]. The model has advantageous simplicity and numerical stability [35–37].

In the numerical model, the grouted rock bolt systems are simulated by four-node bilinear axisymmetric quadrilateral elements with reduced integration (CAX4R). The two-dimensional axisymmetric model was used to simulate the debonding process of rock bolts, and its effectiveness has been verified by the authors in Yu et al. The interface at the loaded end of the concrete is fixed during the test for the boundary condition in the rock bolt-grouted system. On the basis of extensive trials, a mesh size of 2 mm for the rock bolt and cement mortar and a mesh size of 5 mm for the concrete are deemed adequate to obtain sufficiently accurate results. The stiffness matrix is singular when the damage value, scalar stiffness degradation (SDEG), is equal to 1. Therefore, the maximum damage value was limited to 0.9998 to avoid the occurrence of a singular stiffness matrix [38]. The bond strengths between rock bolt, concrete, and cement mortar are 1.57 MPa and 2.16 MPa, respectively. The material parameters of the rock bolt, concrete, and cement mortar are presented in Table 2. We also compare the numerical and experimental results (Figure 2) to validate the numerical model. Both sets of results indicate that the interface between the rock bolt and cement mortar experiences elastic ascending, softening, and debonding stages.

Table 2: Material properties of the rock bolt, concrete, and cement mortar.

Ingredient	Density (kg/m^3)	Elastic modulus (GPa)	Poisson's ratio
Rockbolt	7850	210	0.3
Cement mortar	2035	15.3	0.16
Concrete	2300	33	0.23

Figure 5 shows the rock bolt debonding under different pullout loads. Under 50 kN, the numerical simulation results show that the rock bolt has debonded 632 mm, and the error is 5.5% compared with the test result of 669 mm obtained according to the change in wave velocity, as shown in Figure 3. Therefore, the numerical simulation can well describe the debonding of rock bolts.

The distribution of axial stress in the rock bolt with a defect of 400 mm length (consistent with the test model) under different pullout loads is shown in Figure 6. The axial stress increases with increasing load at the same position. The farther away from the loading end, the smaller the axial stress of the rock bolt under the same load. There is a stress platform at the defect; therefore, the location and length of the defect can be determined according to the distribution law of the axial stress platform of the rock bolt.

4.1.2. Experimental Verification. The cut-off frequency of the guided wave in the grouted rock bolt free of loading was 22 kHz. Therefore, the input waveform of the ultrasonic guided wave was the sine wave with 10 cycles and 22 kHz frequency obtained by the Hanning window (Figure 7) [26]. The comparison between the numerical and experimental results is shown in Figure 8. The signal received at the F-end was in good agreement with the experimental result, which indicated that the numerical model could simulate the guided wave propagation in grouted rock bolt systems.

4.2. The Influence of Different Bond Defect Locations on Guided Wave Propagation.

The axisymmetric model of grouted rock bolt systems with one bond defect at different locations is shown in Figure 9. The model dimensions (except for the defect length and location) were consistent with the specimen in the test. The length of the bond defect was 200 mm, and the distances from the C-end to the B-end were 300 mm, 650 mm, and 1,000 mm.

4.2.1. The Influence of Bond Defect Locations on Guided Wave Propagation without Load. The propagation of the guided wave in the rock bolt with one bond defect at different locations is shown in Figure 10. In Figure 10(a), when the bond defects were at different locations, the echoes of the B-, E-, and F-ends could be received simultaneously at the A-end (the ends of A, B, C, D, E, and F are shown in

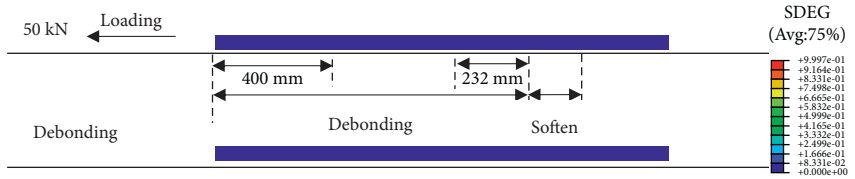

Figure 5: The debonding state under different pullout loads.

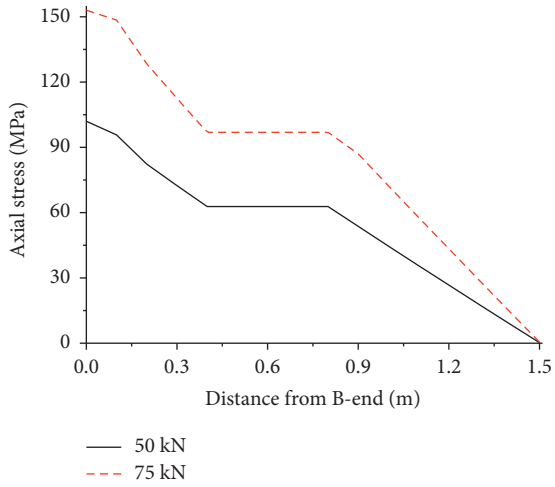

Figure 6: The distribution of axial stress at different grouted positions.

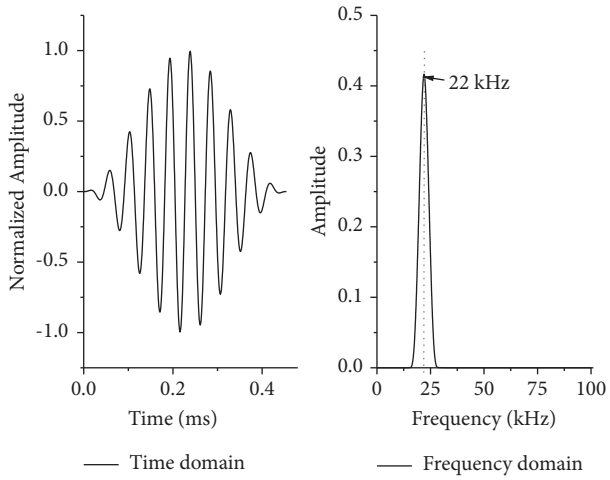

Figure 7: Excitation signal input for the numerical simulation [26].

Figure 9). The farther away from the A-end, the greater the time required for receiving the C-end and D-end echoes at the A-end. In Figure 10(b), the A-end and B-end echoes could be received simultaneously at the F-end, and the location of the bond defect had no effect on it. The closer to the A-end, the greater the time required for receiving the C-end and D-end echoes at the F-end. Therefore, the location and length of the bond defect can be determined by the echo signal propagation time and the guided wave velocity received at the A-end or F-end.

4.2.2. Influence of Pullout Load on Guided Wave Propagation. Under different pullout loads, the axial stress

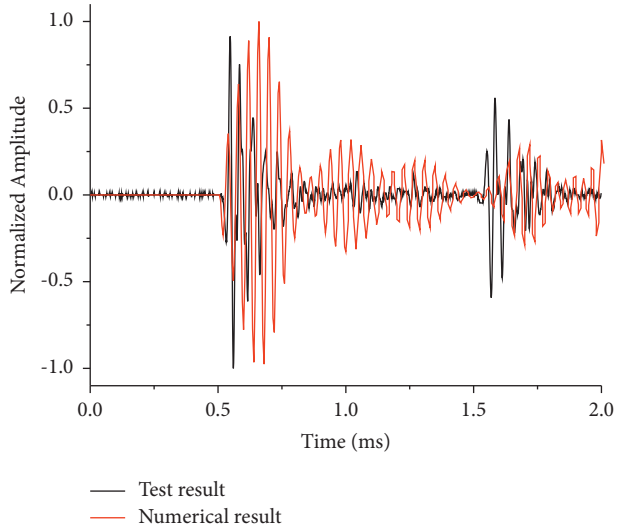

Figure 8: Comparison of numerical and experimental results.

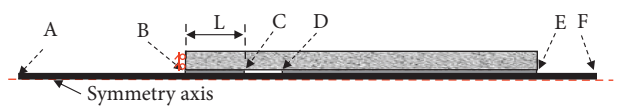

Figure 9: The axisymmetric model of grouted rock bolt systems with one bond defect.

distribution along the rock bolt with a bond defect length of 200 mm is shown in Figure 11. At the same bond defect location, the axial stress in the rock bolt increased with increasing load. Under the same load, for bond defects with the same length and different locations, the axial stress distribution in the rock bolt was independent of the bond defect location except for the stress platform. Therefore, the location of the bond defect could be determined according to the difference in axial stress.

Figure 12 shows the guided wave propagation signal in the rock bolt with a bond defect length of 200 mm and a 300 mm distance from the B-end under different pullout loads. Under a 0 kN load, the propagation regularity of the guided wave was very regular, and the location and size of the bond defect could be obtained by the echo time and wave velocity. However, under loads of 50 and 75 kN, the guided wave propagation signal in the rock bolt was disordered, the rock bolt bore a greater concentrated force at the loading end, and guided waves produced strong multiple reflections. The reflected signal becomes extremely complex, resulting in pullout load disrupting the guided wave propagation and part of the rock bolt debonding. The guided wave energy is interfered with by the generated discontinuous interface,

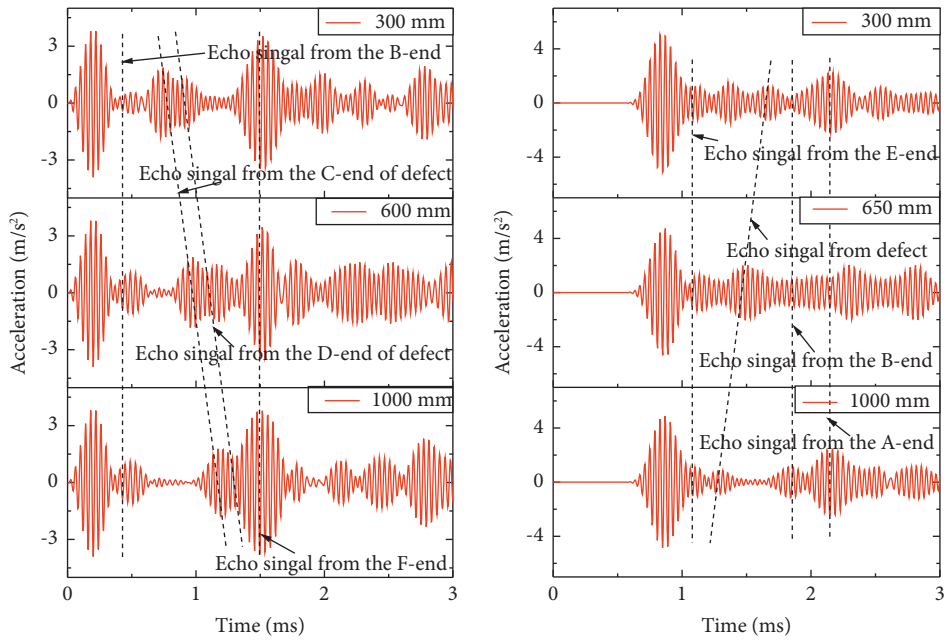

Figure 10: The wave propagation signal in the rock bolt with one bond defect at different locations without load: (a) A-end and (b) F-end.

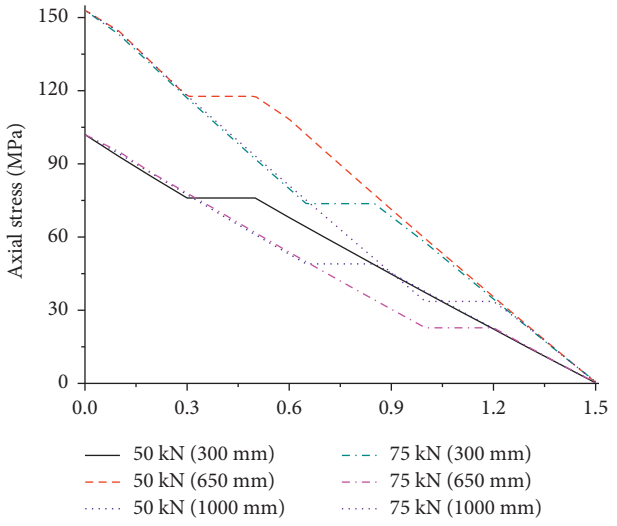

Figure 11: The axial stress distribution along the rock bolt under pullout loads.

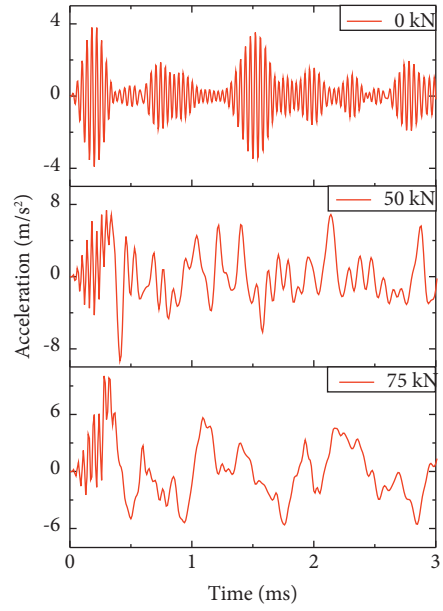

Figure 12: The wave propagation signal in the rock bolt with one bond defect (far away from the B-end 300 mm) under pullout loads.

and part of the energy can only propagate in the rock bolt. The pullout load weakened the propagation law of the guided wave; the larger the pullout load was, the greater the weakening effect.

At the bond defect, the transmission and reflection of the guided wave occurred many times, there was no contact between the rock bolt and cement mortar, the guided wave did not diffract, and all the energy can only spread in the rock bolt, thus affecting the propagation law of the guided wave in the grouted rock bolt systems. In the numerical test, the energy dissipation of the guided wave was serious due to the existence of multiple variable impedance interfaces in the whole grouted range of the rock bolt. Under a pullout load, there was not much guided wave energy diffused into the cement mortar and concrete through the interface between the rock bolt and cement mortar because the wave impedance mismatch increased (the low-frequency impedance mismatch between the rock bolt and cement mortar and the high-frequency impedance mismatch between the rock bolt and air) [39]. In the debonding, there was a gap between the rock bolt and cement mortar. The coupling between cement mortar and air occurs, and the wave impedance is large. There are gaps in the bond defects, and the wave impedance

between cement mortar and the air was large [40], causing guided wave propagation in the rock bolt and multiple reflections in debonding and defects. The propagation velocity of the guided wave in rock bolts was greater than that in cement mortar and concrete, and part of the guided wave scatters more in all directions in cement mortar and concrete, resulting in serious attenuation.

5. Conclusions

In this study, bond defect detection in a fully grouted rock bolt under different pullout loads was tested and numerically simulated. The following conclusions were obtained:

(1) There is a stress platform at the bond defect in grouted rock bolt systems. The location and length of the bond defect can be determined by the stress platform. The pullout test could be used to detect the bond quality of grouted rock bolt systems.

(2) The debonding length of the rock bolt is obtained according to the change in wave velocity in the rock bolt under pullout loads. The amplitude ratios (Q) of low frequency to high frequency were 2.85, 1.92, and 1.72 under 0 kN, 50 kN, and completely debonding conditions, respectively. The rock bolt debonding length increases exponentially with the Q value because of the existence of defects and pullout loads.

(3) In the time-frequency domain, from 0 kN to 50 kN load and until rock bolt complete debonding, the guided wave energy leaked into the cement mortar and concrete decreased, the intensity of the high-frequency band increased and the bond quality deteriorated.

(4) In the numerical test, the guided wave propagation in grouted rock bolt systems with bond defects is irregular due to the existence of multiple variable impedance interfaces in the whole grouted range of rock bolts. Under the pullout load, little guided wave energy diffused into the cement mortar and concrete through the interface between the rock bolt and cement mortar because the wave impedance mismatch between the rock bolt and cement mortar (defect) increased.

Data Availability

The data used to support the findings of this study are included within the article.

Conflicts of Interest

The authors declare no conflicts of interest.

Acknowledgments

This work was funded by the National Science Foundation of China (Grant no. 52104157 and 51904056). These support are gratefully acknowledged.

References

[1] A. Bobet and H. H. Einstein, "Tunnel reinforcement with rockbolts," *Tunnelling and Underground Space Technology*, vol. 26, no. 1, pp. 100–123, 2011.

[2] Y. M. Zhao and M. J. Yang, "Pull-out behavior of an imperfectly bonded anchor system," *International Journal of Rock Mechanics and Mining Sciences*, vol. 48, no. 3, pp. 469–475, 2011.

[3] C. Xu, Z. H. Li, S. Y. Wang, S. Wang, L. Fu, and C. Tang, "Pullout performances of grouted rockbolt systems with bond defects," *Rock Mechanics and Rock Engineering*, vol. 51, no. 3, pp. 861–871, 2018.

[4] F. Xu, K. Wang, S. G. Wang, W. W. Li, W. Q. Liu, and D. S. Du, "Experimental bond behavior of deformed rebars in half-grouted sleeve connections with insufficient grouting defect," *Construction and Building Materials*, vol. 185, pp. 264–274, 2018.

[5] Y. Cui and D. H. Zou, "Assessing the effects of insufficient rebar and missing grout in grouted rock bolts using guided ultrasonic wavesficient rebar and missing grout in grouted rockbolts using guided ultrasonic waves," *Journal of Applied Geophysics*, vol. 79, pp. 64–70, 2012.

[6] C. Q. Fang, K. Lundgren, L. G. Chen, and C. Y. Zhu, "Corrosion influence on bond in reinforced concrete," *Cement and Concrete Research*, vol. 34, no. 11, pp. 2159–2167, 2004.

[7] F. Tondolo, "Bond behaviour with reinforcement corrosion," *Construction and Building Materials*, vol. 93, pp. 926–932, 2015.

[8] P. Craig, S. Serkan, P. Hagan et al., "Investigations into the corrosive environments contributing to premature failure of Australian coal mine rockbolts," *International Journal of Mining Science and Technology*, vol. 26, no. 1, pp. 59–64, 2016.

[9] L. P. Srivastava and M. Singh, "Effect of fully grouted passive bolts on joint shear strength parameters in a blocky mass," *Rock Mechanics and Rock Engineering*, vol. 48, no. 3, pp. 1197–1206, 2015.

[10] L. P. Srivastava and M. Singh, "Empirical estimation of strength of jointed rocks traversed by rockbolts based on experimental observation," *Engineering Geology*, vol. 197, pp. 103–111, 2015.

[11] W. Nie, Z. Y. Zhao, S. Q. Ma, and W. Guo, "Effects of joints on the reinforced rock units of fully-grouted rockbolts," *Tunnelling and Underground Space Technology*, vol. 71, pp. 15–26, 2018.

[12] C. S. Zhang, D. H. Zou, and V. Madenga, "Numerical simulation of wave propagation in grouted rockbolts and the effects of mesh density and wave frequency," *International Journal of Rock Mechanics and Mining Sciences*, vol. 43, no. 4, pp. 634–639, 2006.

[13] L. D. Suits, T. C. Sheahan, S. I. Han, I. M. Lee, Y. J. Lee, and J. S. Lee, "Evaluation of rockbolt integrity using guided ultrasonic waves," *Geotechnical Testing Journal*, vol. 32, no. 1, pp. 101311–101338, 2009.

[14] I. M. Lee, S. I. Han, H. J. Kim, J. D. Yu, B. K. Min, and J. S. Lee, "Evaluation of rockbolt integrity using Fourier and wavelet transforms," *Tunnelling and Underground Space Technology*, vol. 28, pp. 304–314, 2012.

[15] J. D. Yu, M. H. Bae, I. M. Lee, and J. S. Lee, "Nongrouted ratio evaluation of rockbolts by reflection of guided ultrasonic waves," *Journal of Geotechnical and Geoenvironmental Engineering*, vol. 139, no. 2, pp. 298–307, 2013.

[16] J. D. Yu, Y. H. Hong, Y. H. Byun, and J. S. Lee, "Non-destructive evaluation of the grouted ratio of a pipe roof support system in tunneling," *Tunnelling and Underground Space Technology*, vol. 56, pp. 1–11, 2016.

[17] B. Zima and M. Rucka, "Non-destructive inspection of ground anchors using guided wave propagation," *International Journal of Rock Mechanics and Mining Sciences*, vol. 94, pp. 90–102, 2017.

[18] B. Zima and M. Rucka, "Guided ultrasonic waves for detection of debonding in bars partially embedded in grout," *Construction and Building Materials*, vol. 168, pp. 124–142, 2018.

[19] T. Stepinski, "Novel instrument for inspecting rockbolt integrity using ultrasonic guided waves," *Measurement*, vol. 177, Article ID 109271, 2021.

[20] Z. Li, J. G. Yu, X. M. Zhang, and L. Elmaimouni, "Theoretical and Experimental Study on Guided Wave Characteristics in Bonded Bolts," *Mechanics Of Advanced Materials And Structures*, vol. 2022, Article ID 2070802, 2022.

[21] M. C. He, H. P. Xie, S. P. Peng, and Y. D. Jiang, "Study on rock mechanics in deep mining engineering," *Chinese Journal of Rock Mechanics and Engineering*, vol. 24, no. 16, pp. 2803–2813, 2005.

[22] G. Stjern and A. Myrvang, "The influence of blasting on grouted rockbolts," *Tunnelling and Underground Space Technology*, vol. 13, no. 1, pp. 65–70, 1998.

[23] A. Ivanovic, R. D. Neilson, and A. A. Rodger, "Influence of prestress on the dynamic response of ground anchorages," *Journal of Geotechnical and Geoenvironmental Engineering*, vol. 128, no. 3, pp. 237–249, 2002.

[24] A. Ivanovic and R. D. Neilson, "Non-destructive testing of rockbolts for estimating total bolt length," *International Journal of Rock Mechanics and Mining Sciences*, vol. 64, pp. 36–43, 2013.

[25] S. S. Yu, W. C. Zhu, L. L. Niu, S. C. Zhou, and P. H. Kang, "Experimental and numerical analysis of fully grouted long rockbolt load-transfer behavior," *Tunnelling and Underground Space Technology*, vol. 85, pp. 56–66, 2019.

[26] S. S. Yu, W. C. Zhu, and L. L. Niu, "Experimental and numerical evaluation on debonding of fully grouted rockbolt under pull-out loading," *International Journal of Coal Science & Technology*, vol. 9, no. 1, pp. 8–15, 2022.

[27] Y. Li, C. S. Zhang, and C. Wang, "Study on several key issues in nondestructive detection of bolt bonding integrity," *Chinese Journal of Rock Mechanics and Engineering*, vol. 27, no. 1, pp. 108–116, 2008.

[28] B. Sun, X. T. Zheng, S. Zeng, Z. F. Chen, and S. S. Guo, "Multi-scale analysis on anchoring defects diagnosis under multiple measuring points," *Journal of China Coal Society*, vol. 39, no. 7, pp. 1385–1390, 2014.

[29] H. P. Niu, *Estimating the Quality of Grouted Rockbolts Using Ultrasonic Waves in Rock Mass*Taiyuan University of Technology, Taiyuan China, 2012.

[30] K. I. Song and G. C. Cho, "Bonding state evaluation of tunnel shotcrete applied onto hard rocks using the impact-echo method," *NDT&E International*, vol. 42, no. 6, pp. 487–500, 2009.

[31] G. Trtnik and M. Gams, "The use of frequency spectrum of ultrasonic P-waves to monitor the setting process of cement pastes," *Cement and Concrete Research*, vol. 43, pp. 1–11, 2013.

[32] F. Yao, G. Y. Chen, and A. Abula, "Research on signal processing of segment-grout defect in tunnel based on impact-echo method," *Construction and Building Materials*, vol. 187, pp. 280–289, 2018.

[33] J. Lee and G. L. Fenves, "Plastic-damage model for cyclic loading of concrete structures," *Journal of Engineering Mechanics*, vol. 124, no. 8, pp. 892–900, 1998.

[34] Dassault Systemes Simulia, *ABAQUS Theory Manual & Users Manuals Version 6.11*, USA, 2014.

[35] P. Z. Qiao and Y. Chen, "Cohesive fracture simulation and failure modes of FRP–concrete bonded interfaces," *Theoretical and Applied Fracture Mechanics*, vol. 49, no. 2, pp. 213–225, 2008.

[36] J. Henriques, L. Simões da Silva, and I. B. Valente, "Numerical modeling of composite beam to reinforced concrete wall joints part1: calibration of joint components," *Engineering Structures*, vol. 52, pp. 747–761, 2013.

[37] J. Henriques, L. Simões da Silva, and I. B. Valente, "Numerical modeling of composite beam to reinforced concrete wall joints: Part II: global behavior," *Engineering Structures*, vol. 52, pp. 734–746, 2013.

[38] W. R. Yang, X. J. He, and L. Dai, "Damage behaviour of concrete beams reinforced with GFRP bars," *Composite Structures*, vol. 161, pp. 173–186, 2017.

[39] K. I. Song and G. C. Cho, "Numerical study on the evaluation of tunnel shotcrete using the impact-echo method coupled with Fourier transform and short-time Fourier transform," *International Journal of Rock Mechanics and Mining Sciences*, vol. 47, no. 8, pp. 1274–1288, 2010.

[40] T. Yu, J. F. Chaix, L. Audibert, D. Komatitsch, V. Garnier, and J. M. Hénault, "Simulations of ultrasonic wave propagation in concrete based on a two-dimensional numerical model validated analytically and experimentally," *Ultrasonics*, vol. 92, pp. 21–34, 2019.